# Studies on Thin Liquid Film of Annular-mist Two-phase Flow : I. Wave Characteristics and Heat Transfer

AUTHOR(S):

HAGIWARA, Yoshimichi; SUZUKI, Kenjiro; SATO, Takashi

CITATION:

HAGIWARA, Yoshimichi ...[et al]. Studies on Thin Liquid Film of Annular-mist Two-phase Flow : I. Wave Characteristics and Heat Transfer. Memoirs of the Faculty of Engineering, Kyoto University 1982, 44(2): 309-328

ISSUE DATE:

1982-06-30

URL:

http://hdl.handle.net/2433/281215

# Studies on Thin Liquid Film of Annular-mist Two-phase Flow I. Wave Characteristics and Heat Transfer

By

Yoshimichi HAGIWARA, Kenjiro SUZUKI and Takashi SATO*

(Received December 26, 1981)

**Abstract**

This paper presents measurements both of the heat transfer coefficient and wave characteristics of liquid film in an annular-mist two-phase two component flow. The liquid film surface waves were obtained by a two-wire conductance method. Comparing the increasing tendency of the heat transfer coefficient on the liquid flow rate with that of the wave height, the enhancement of the heat transfer coefficient is found to correspond to the onset of disturbance waves. Additionally, the relationship between the wave velocity and its height was obtained, using two sets ofconductance probes. The velocity of ripple increases with its height, while the velocity of disturbance wave increases with apparent gas phase velocity, regardless of its height.

## Nomenclature

| | |
|---|---|
| $a$ | thermal diffusivity |
| $c$ | velocity of liquid film surface wave |
| $D$ | pipe diameter of test section |
| $f$ | wave frequency |
| $G$ | mass flow rate |
| $p$ | film thickness probability |
| $pdf$ | probability density function of wave height |
| $q$ | heat flux |
| $T$ | temperature |
| $t$ | time |
| $U$ | axial mean velocity |
| $x$ | axial coordinate |
| $y$ | coordinate perpendicular to the pipe wall |
| *Greek* | |
| $\alpha$ | heat transfer coefficient |

* Department of Mechanical Engineering

$\delta$ liquid film thickness
$\lambda$ thermal conductivity
$\nu$ Kinematic viscosity
$\pi$ 3.14159.....
$\rho$ density
$\tau$ shear stress
$\theta$ temperature difference

*Subscripts*

$B$ base film
$CL$ centerline
$DW$ condition of appearing disturbance wave
$g$ gas phase
$l$ liquid phase
$max$ maximum
$M$ mixing or uniform state
$R$ condition of appearing ripple
$w$ wall
0 apparent

*Superscripts*

$+$ dimensionless
$-$ average

## 1. INTRODUCTION

Annular two-phase flow is encountered in many practical heat and mass transfer systems, in boiling tube flow at high quality, in the condensation process in a tube, in some chemical engineering devices, in heat pipe and so on. Interactions between gas phase flow and liquid phase flow occur at their interface in any gas-liquid two-phase flow systems. One of the typical interactions found in the annular flow regime is the onset of waves at the interface. The waves in turn affect the heat, mass and momentum transfer in a tube. Doubtlessly, therefore, a detailed study of the wave structure is of practical importance, and from this view point many studies have been made so far on the wave characteristics[1)~4)]. However, present knowledge of the wave structure is still felt from sufficient because of its complex features, especially when the liquid film is not so thick.

The usual theoretical approaches to the annular flow heat transfer treat the wave effect very simply in an implicit way[5),6)]. The interface shear stress or the axial pressure gradient to be affected by the structure of the waves is introduced, and is evaluated from some empirical relationship, for example, from the formula expressed

in terms of the Lockhart-Martinelli parameter. This may reflect the lack of comprehensive knowledge about the wave structure. The above cited studies are concerned with thick liquid film so that the liquid film is presumed to be turbulent. In regard to the interactive effects of waves and turbulence, waves have been reported to suppress the intrinsic turbulence near the interface in the liquid film[7]. If this is true under any condition, the critical liquid film Reynolds number for the laminar-to-turbulent transition should be higher, and thin liquid film is liable to remain laminar. However, as is well-known,in condensation heat transfer, the Nusselt number is higher than the laminar flow value in the intermediate range of liquid film Reynolds number, and shows the Reynolds number dependency to be quite different from that in the laminar condition. This is sometimes ascribed to the turbulent effect, but is in contradiction with the above mentioned higher critical Reynolds number. Detailed study has to be made to get a deeper insight into the wave structure and its effect.

The present experiment aims not only at studying wave characteristics or its structural parameters, but also at clarifying the wave effects on heat transfer. Therefore, the heat transfer measurement is also reported. To make the wave studies reliable and to facilitate several experimental approaches, an air-water annular two-phase flow is used for the test flow in this experiment. From the heat transfer view point, this is classified as a two-component annular two-phase flow. Similar heat transfer problems have been attacked experimentally by Johnson and Abou-Sabe[8], Groothuis and Hendal[9], Kudirka et al.[10] and Pletcher and McManus[11], and theoretically by McManus and Pletcher[12]. All of these are for the thick liquid film, and some of them are for the horizontal tube. The present study is concerned with the vertical annular flow with thin liquid film whose Reynolds number is much lower than its critical value. To avoid complexity, the wall heat flux is kept low, so that vaporization at the interface does not affect the flow pattern nor the turbulence in the gas phase core flow.

## 2. EXPERIMENTAL PROCEDURE

### 2.1 Apparatus

The flow system used in this study is shown in Figure 1. It is almost the same as that used previously in the study of mist flow,[13] except for the test section. Air is supplied as a gas phase fluid by a compressor 1. Its main portion comes into the test section through the pipe 6. The remaining portion is issued from the atomizer 11. Both air flow rates are measured separately with orifice flow meters 4 and 8. The total mass flow rate of air in the test section was also confirmed from the measurement of the mean velocity distribution. The velocity distribution was obtained by a Pitot tube traversed in a test section. The air flow temperature was measured with

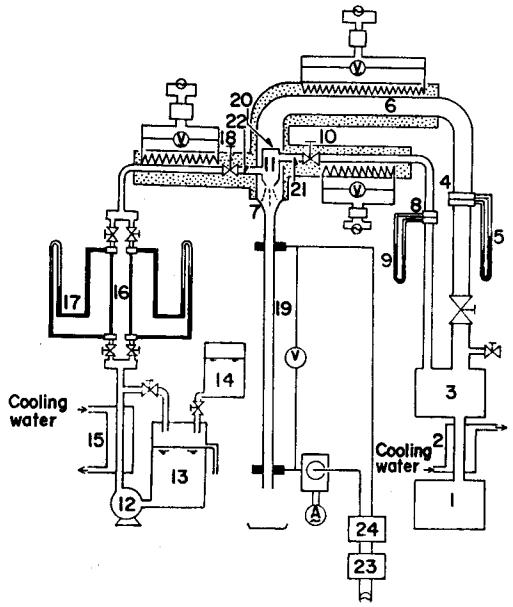


Fig. 1 Flow system

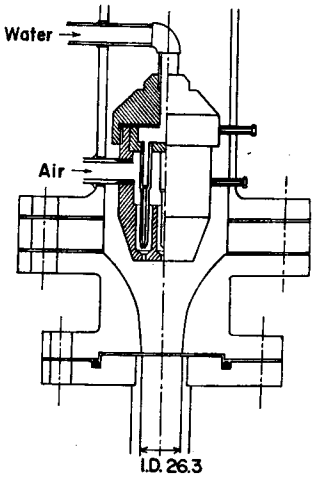


Fig. 2 Detail of atomizer

thermocouples, 20 and 21, located downstream of the orifice flow meters and just before the atomizer.

Clean water is supplied as a liquid phase fluid by a stainless steel pump 12 to the atomizer. The water flow rate was measured with a capillary flow rate meter 16. The water flow temperature was measured also by thermocouples at the position just before the flow rate meter and the atomizer 22.

The temperature of each phase fluid was adjusted by the preheating section located upstream of the atomizer. Each preheating section consists of Nichrome wire and a step-down transformer.

The atomizer used consists of seven small air-atomizers equally spaced and axi-symmetrically allocated. It is mounted at the top of the test section in a way seen in Figure 2. Annular liquid film is mainly formed at the contraction nozzle 7, and it gradually thickens a little as it flows down the test section.

## 2.2 Study on heat transfer coefficient

Figure 3 shows the details of the heating test section. The test section is made up of a seamless 18-8 stainless steel pipe of 26.3 mm inner diameter, 1.0 mm thickness and 1650 mm length. Its inner surface had been previously polished with waste cloths dipped in chemical polishing material. The outer surface of the test section is covered with a glass wool insulator to reduce the thermal leakage to a negligible level.

Chromel-Alumel thermocouples were welded on the outer surface of the heated pipe along the pipe axis at every 50 mm after the location of $x=200$ mm downstream of the outlet of the contraction nozzle. The local outer-wall temperature was obtained by measuring the thermo-electromotive forces of these thermocouples with a digital voltmeter. The local inner-wall temperature was estimated using this outer-wall temperature, and solving the one-dimensional heat conduction equation for a cylinder with internal heat generation. The axi-symmetricity of the flow was checked with other thermocouples welded along the periphery at four axial positions, $x=200$, 600, 1000 and 1400 mm.

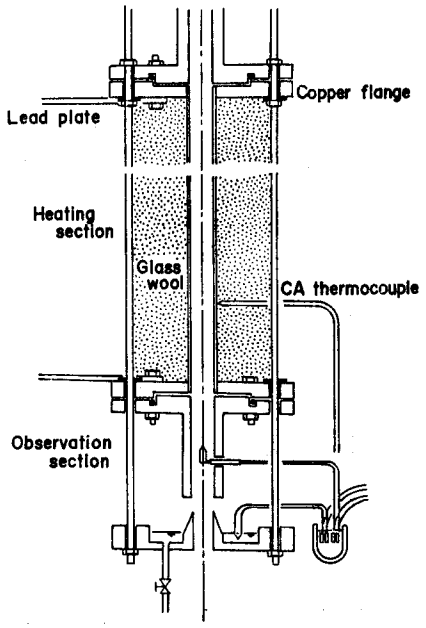


Fig. 3 Detail of heating test section

The observation sections were connected just upstream and downstream of the test section to confirm the flow pattern of the liquid film. Both sections are made up of transparent polycarbonate pipes of 100 mm length. It also helps to insulate the axial flows of the heat and electric currents.

Under the outlet of the test section, the capturing device was set to confirm the liquid film flow rate or evaporation fraction of the liquid phase.

The electrical power input to the heating test section is determined from the measurement of the voltage drop and the current across the section. The first and second transformers, 23 and 24 in Figure 1, are used to reduce the voltage of the commercial alternative electric current in order to adjust the power input.

### 2.3 Study of wave characteristics

The instantaneous liquid film thickness was obtained using a two-wire conductance probe similar to that used by Brown[14] and Tsiklauri et al.[15]. This is composed of two stainless steel fine wires mounted on the inner surface of the test tube, perpendicularly to the surface and spaced 2.5 mm circumferentially.

Figure 4 shows the signal processing circuits. The high frequency electric current of 20 kHz was imposed between the two wires. This level of frequency is high enough to avoid any polarizing action of the liquid between the wires. The electric current conducted through the liquid between the wires was rectified and filtered. The signal finally obtained was recorded and analyzed afterwards. To ensure the linear

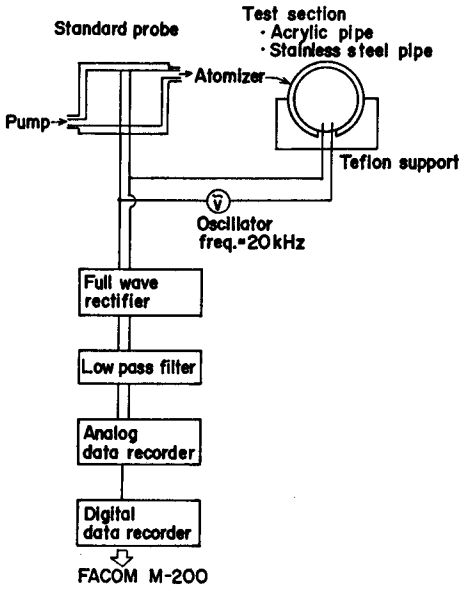


Fig. 4 Record circuit of film thickness

relationship between the film thickness and the magnitude of the signal, the method of Villeneuve[16] was adopted. For this purpose, a standard probe was inserted between the needle valve 18 and the atomizer 11 in Figure 1. In a static calibration experiment, this method proved to be effective. The calibration was made in a shallow open channel. The output signal of the conductance probe mounted on the bottom surface of the channel was compared with a film thickness measured by the needle contact method. Another advantage of this method is that the relationship obtained in the calibration does not vary with liquid property. The results of this proof are shown in Figure 5.

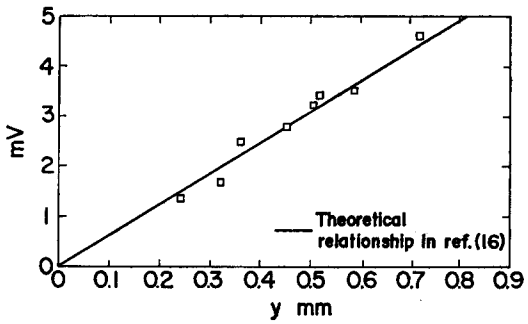


Fig. 5 Proof of linear relationship

The conductance probe was located at $x=1200$ mm, where the flow is developed almost at any flow rate condition.

Some statistical results, such as the film thickness probability, the probability density function of the wave height and the wave frequency, were obtained by passing the output signal of the conductance probe through some suitable electronic circuits or processing it with a digital computer.

The velocity of the liquid film surface wave was determined by using two sets of the above conductance probe. Another conductance probe was located at $x=1220$ mm, 20 mm apart from the first one in the flow direction. The final output signals from the both probes were digitized at the sampling frequency of 2 kHz. The wave velocity was estimated from the time difference found between the corresponding

crests appearing in each digital signal, taking account of the distance between the two sets of probes.

### 2.4 Experimental condition

The gas phase mass flow rates tested are 11.5 g/sec, 15.5 g/sec and 21.1 g/sec. They correspond to the gas phase Reynolds number $Re_g=3.0\times10^4$, $4.0\times10^4$ and $5.5\times10^4$. Therefore, the gas phase flow is fully turbulent. The mass flow rate of the liquid phase is changed from 3.33 g/sec to 11.7 g/sec. It covers the flow regime ranging from the formation of the thin liquid film to the onset of the disturbance wave. In this flow regime, the entrainment of the droplets from the crest of the disturbance wave can be ignored[17]. The liquid film Reynolds number is much lower, such that the liquid film is not considered to be turbulent. In this description, the wave-induced turbulent like motion in the liquid film has been discriminated from the turbulence caused by the intrinsic instability.

The heat flux is restricted within the range of 0.96~2.0 kW/m$^2$. The temperature difference between the pipe wall and the gas phase flow is also restricted to below 20 degree, so that the mass fraction of the water vapour is believed to be low enough at any location. In another study to see the effects of heat flux, the heat flux was nearly doubled.

The measurement with the conductance probes was carried out mainly under an unheated condition. For this purpose, the stainless steel heating pipe explained previously, was replaced by an acrylic pipe of the same size. The results of the unheated wave measurement may be used as the flow data for the analysis of the heat transfer data at a low heat flux, because little temperature variation occurs then in the flow direction. Several measurements were performed under heated conditions. The obtained data are available to estimate the heat flux effects on the wave characteristics.

## 3. EXPERIMENTAL RESULTS

### 3.1 Surface wave characteristics

Figure 6-1 shows some typical examples of the film thickness-time records. The film thickness probability $p$, obtained from several typical liquid flow rate conditions, is seen in Figure 7-1. From these results, the base film thickness $\delta_B$ and the maximum film thickness $\delta_{max}$ can be determined as the distances from the wall to the position where $p=0.99$ and to the position where $p=0.01$, respectively. (See Figure 8) Additionally, the mean film thickness $\bar{\delta}$ can be determined in a way shown in Figure 8. It is given as the value of y where the two hatched areas have the same area.

As seen from Figure 7-1, $\delta_{max}$ and $\bar{\delta}$ increase with the liquid flow rate, while $\delta_B$ does not change remarkably. This means that an increase in the liquid flow rate contributes mainly to the generation of larger amplitude waves.

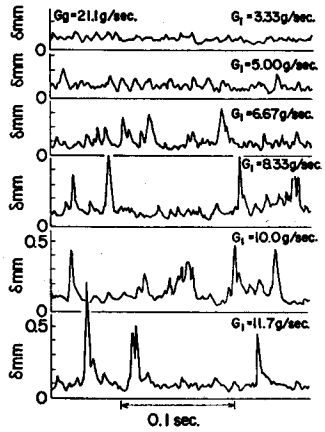


Fig. 6-1 a

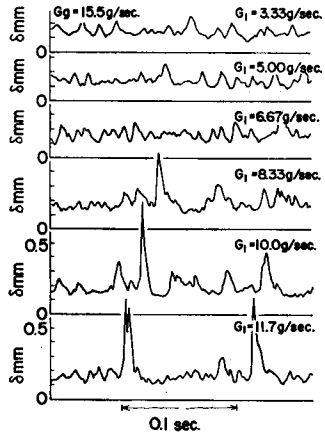


Fig. 6-1 b

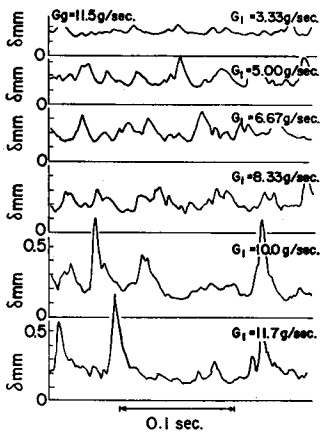


Fig. 6-1 c

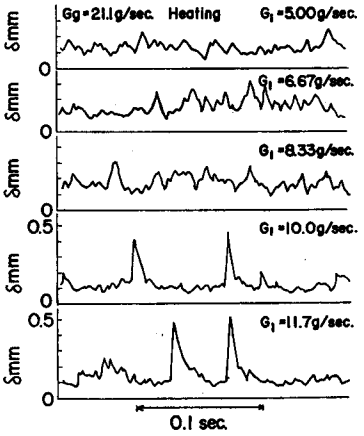


Fig. 6-2 a

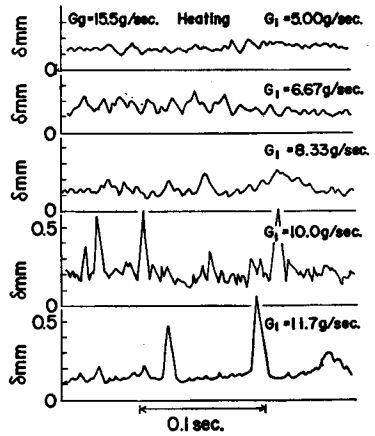


Fig. 6-2 b

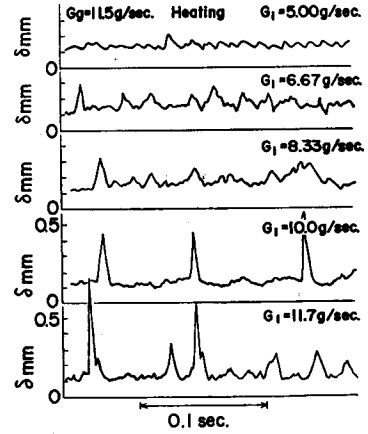


Fig. 6-2 c

Fig. 6 Typical examples of film thickness-time records

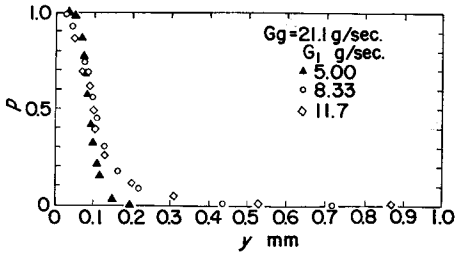


Fig. 7-1 a

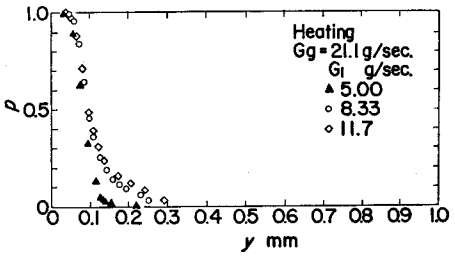


Fig. 7-2 a

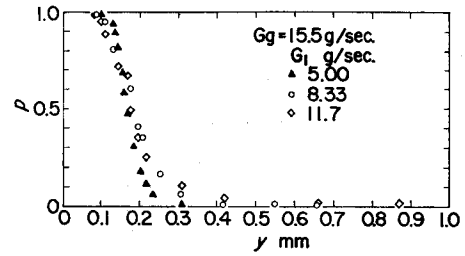


Fig. 7-1 b

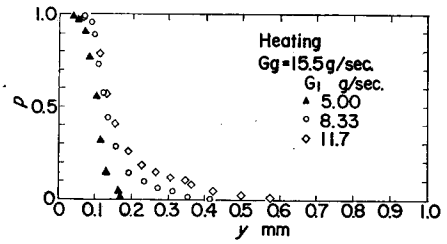


Fig. 7-2 b

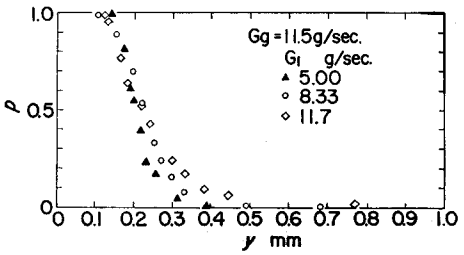


Fig. 7-1 c

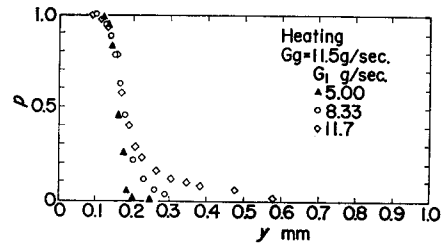


Fig. 7-2 c

Fig. 7 Film thickness probability

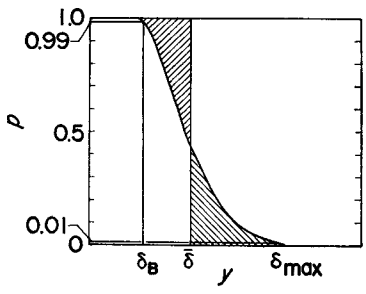


Fig. 8 Definition of film thickness

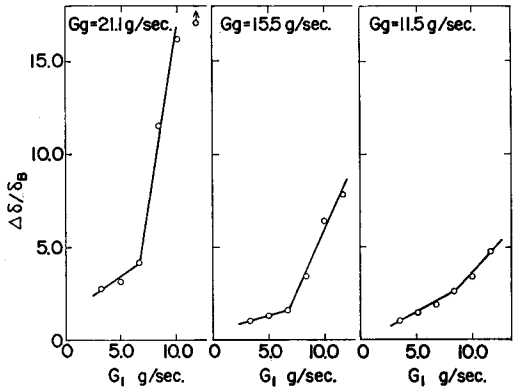


Fig. 9 Increasing tendency of maximum wave amplitude with liquid flow rate

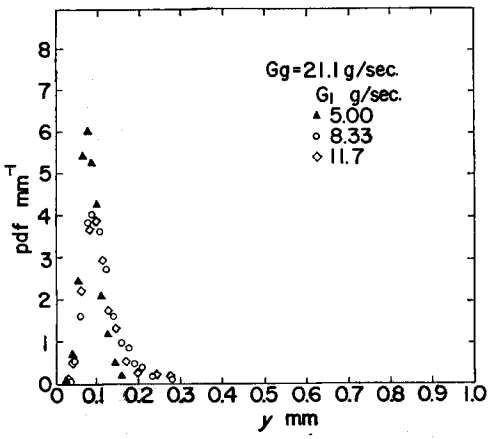


Fig. 10-1 a

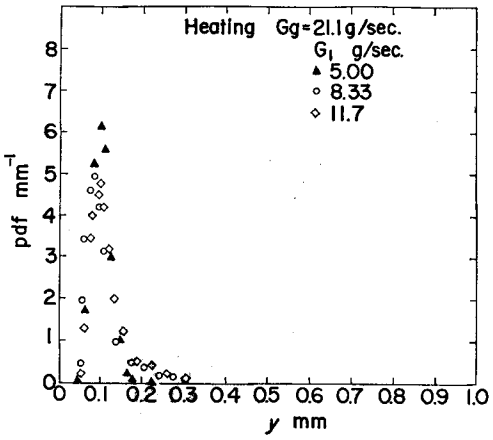


Fig. 10-2 a

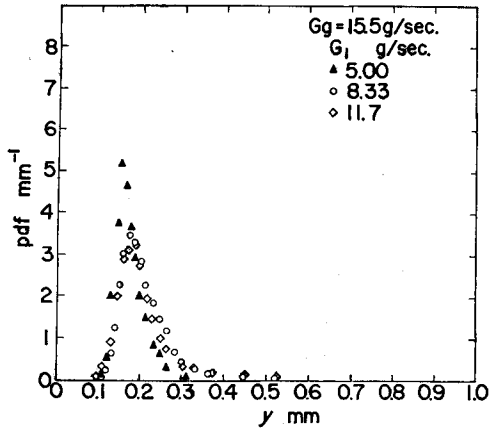


Fig. 10-1 b

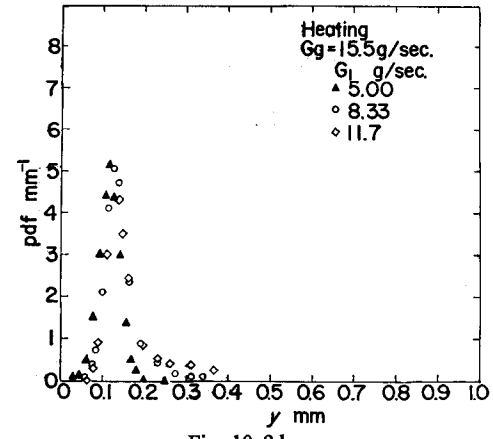


Fig. 10-2 b

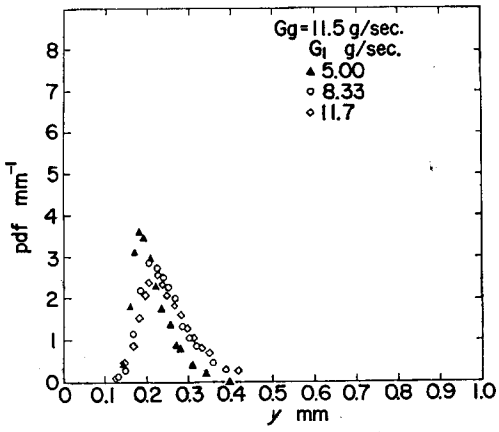


Fig. 10-1 c

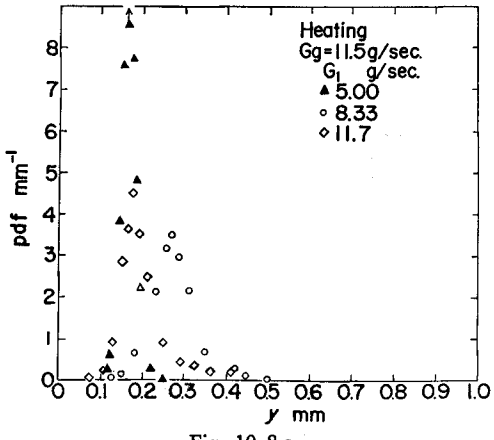


Fig. 10-2 c

Fig. 10 Probability density function of wave height

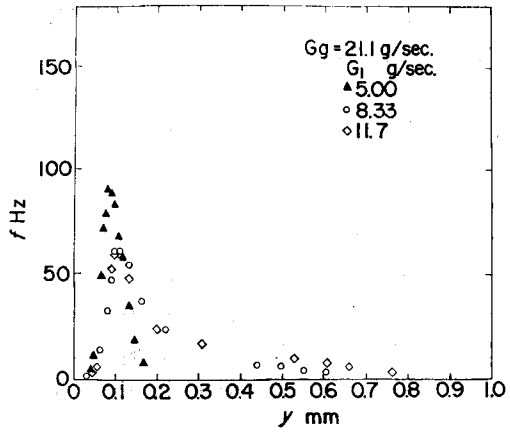


Fig. 11-1 a

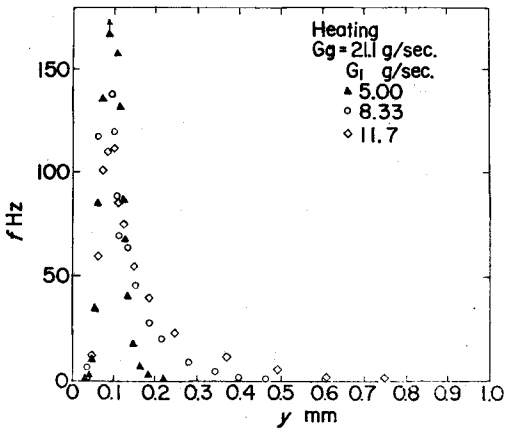


Fig. 11-2 a

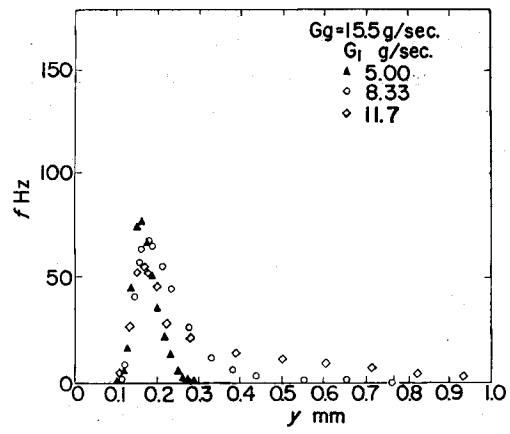


Fig. 11-1 b

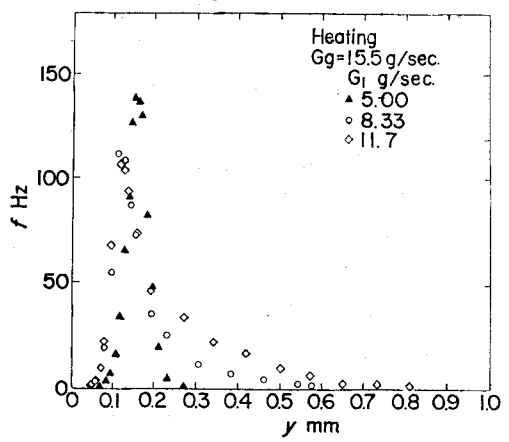


Fig. 11-2 b

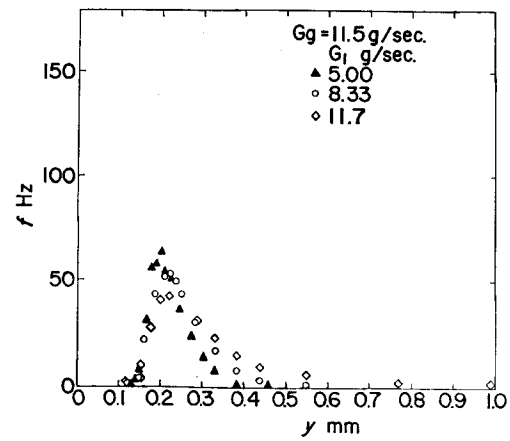


Fig. 11-1 c

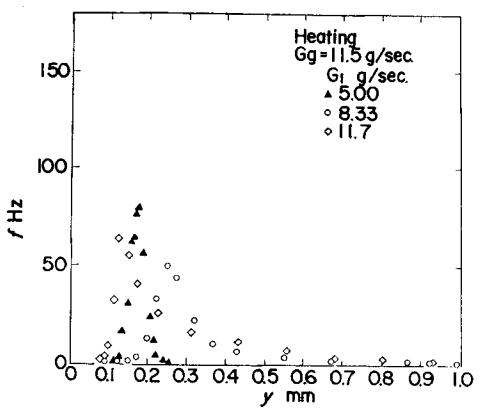


Fig. 11-1 c

Fig. 11 Wave frequency

In the case of high liquid flow rate conditions, i.e. $G_l=10.0$ g/sec and 11.7 g/sec, the disturbance waves appear in Figure 6-1. To confirm the onset of the disturbance wave, the dependence of the maximum wave amplitude $\Delta\delta=\delta_{max}-\delta_B$ on the liquid flow rate was plotted in Figure 9. In this Figure, a sudden change occurs in the increasing tendency of the maximum amplitude with the liquid flow rate. This may correspond to the onset of the disturbance wave in Figure 6-1.

Figure 10-1 shows the probability density function of the wave height. The nearly normal distribution around the mean film thickness shows the existence of random height waves in the lower flow rate condition, i.e. the ripple wave. When the liquid flow rate increases, the probability density function is distorted. This corresponds to the appearance of disturbance waves. Similar trends are also seen in the wave frequency $f$. (See Figure 11-1)

### 3.2 Disturbance wave frequency

It is intended here to distinguish the disturbance wave from the other waves. One of the most typical characteristics of the disturbance wave is the rapid increase of its height with the elapse of time. Thus, the disturbance waves are expected to be detected if a threshold is set for the time derivative of the film thickness signal. With this criterion, a conditional sampling was applied to the signal.

The disturbance wave frequency $f_{DW}$ was determined by conting the number of waves sampled with the above criterion. The suitable threshold level was determined so as to obtain $f_{DW}$ independent on the threshold adopted. Then the final values of the threshold level and the disturbance wave frequency were ultimately determined. Additionally, it was confirmed at the same time, that no wave meeting the above criterion was found in the low flow rate condition, i.e. the ripple flow regime. The disturbance wave frequency obtained is shown in Figure 12. $f_{DW}$ slightly increases with the averaged gas phase velocity $U_{Og}$.

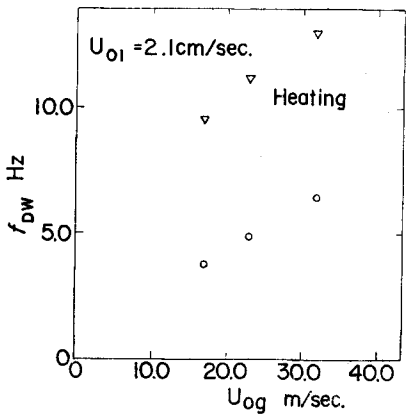


Fig. 12 Disturbance wave frequency

### 3.3 Wave velocity

The relation between the wave height and wave velocity obtained from the digitized signal is seen in Figure 13. The disturbance wave data which satisfy the criterion mentioned in 3.2 are located above the broken lines in the Figure. The higher the ripple wave is, the faster it is propagated, irrespective of the existence of the disturbance wave. On the other hand, the velocity of the disturbance wave is much higher than that of the ripple wave, and seems to vary little with the wave

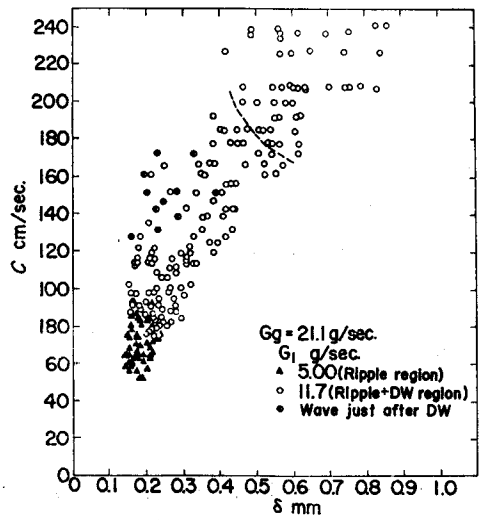


Fig. 13-a

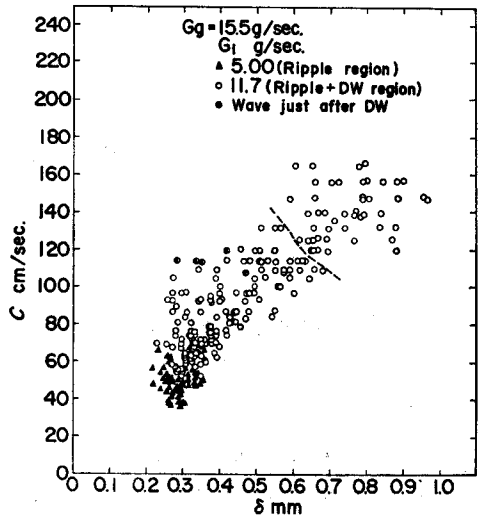


Fig. 13-b

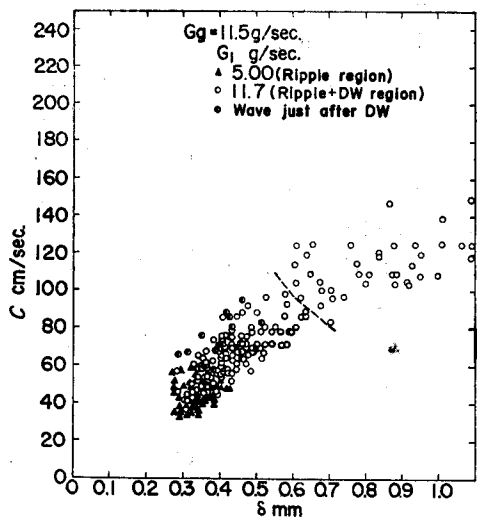


Fig. 13-c

Fig. 13 Relationship between wave height and wave velocity

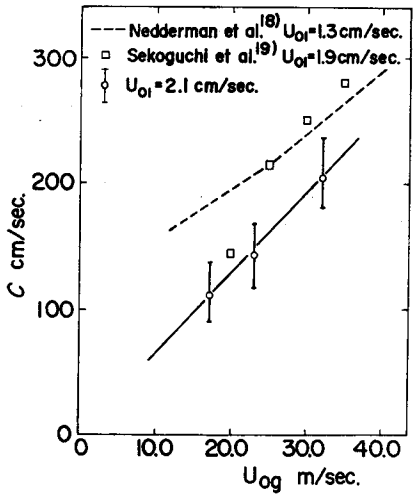


Fig. 14 Dependency of disturbance wave velocity on apparent gas phase velocity

height. The averaged velocity of the disturbance wave increases proportionally with the apparent velocity of the gas phase, as seen in Figure 14. Similar trends can be seen in reference[18),19)].

### 3.4 Heat transfer coefficient

The distribution of the local heat transfer coefficient $\alpha$ is shown in Figure 15-1. The abscissa is the dimensionless streamwise location, the distance $x$ divided by the pipe diameter $D$. The heat transfer coefficient is defined, based on the temperature difference between the wall temperature and the local centerline fluid temperature $T_{CL}$. $T_{CL}$ has actually been evaluated by assuming the linear distribution between the inlet, $x=0$ and the position, $x=1800$ mm, close to the outlet.

In the region of $x/D<40$ in Figure 15-1, the heat transfer coefficient $\alpha$ decreases downstream, because both the temperature - and the velocity distributions are 'developing'. In the region of $x/D>40$, however, the coefficient does not change remarkably, where the temperature distribution is estimated as being almost 'developed' as well as the velocity distribution.

When the liquid flow rate exceeds a certain value, $\alpha$ decreases downstream more gradually and approaches a higher level. To confirm this change, the values of $\alpha$ at the fixed positions, $x=800$, 1200 and 1500 mm, are plotted against the liquid flow rate, as shown in Figure 16. Comparing Figure 16 with Figure 9, the onset of disturbance waves just corresponds to the change of tendency of the heat transfer coefficient. Therefore, it can be explained that the onset of the disturbance waves causes the enhancement of heat transfer.

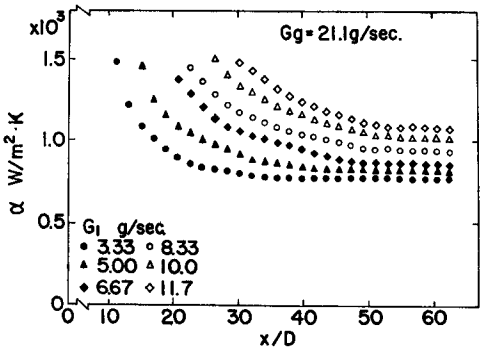


Fig. 15-1 a

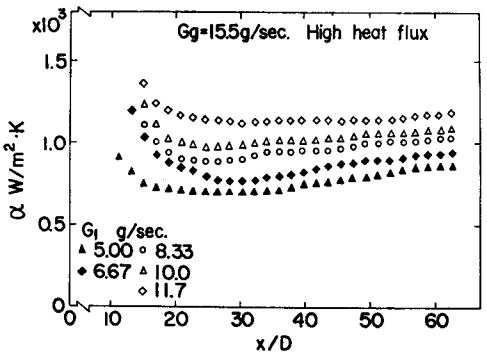


Fig. 15-2 a

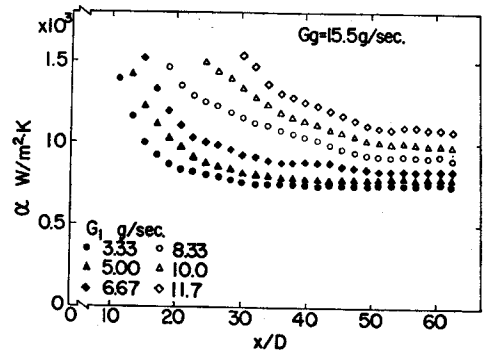


Fig. 15-1 b

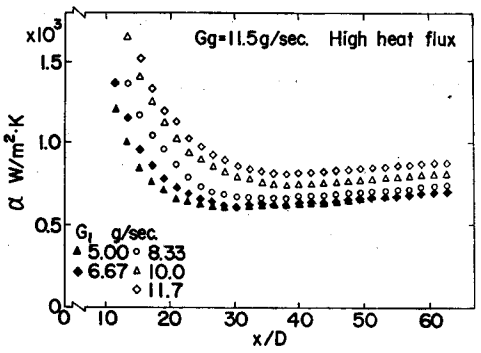


Fig. 15-2 b

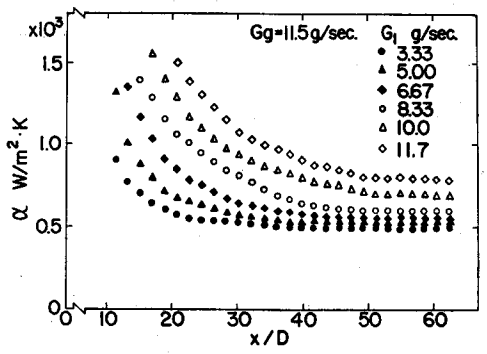


Fig. 15-1 c

Fig. 15 Heat transfer coefficient

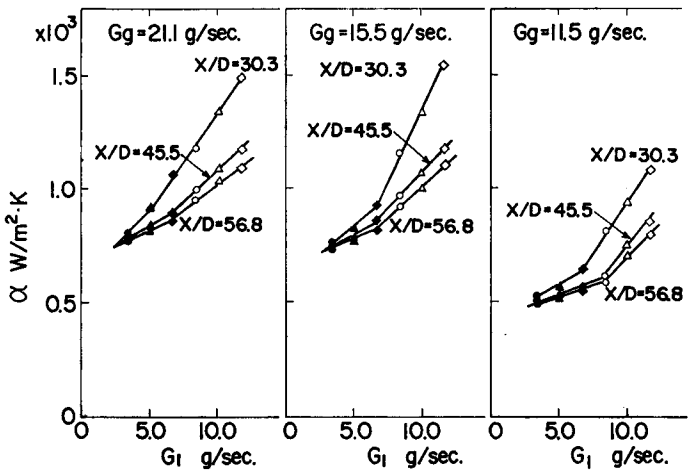


Fig. 16 Increasing tendency of heat transfer coefficient with liquid flow rate

### 3.5 Effects of heat flux

Figure 7-2 shows the film thickness probability $p$ obtained in the case of a higher heat flux. Although all of the film thickness parameters, $\delta_B$, $\bar{\delta}$ and $\delta_{max}$, estimated from Figure 7-2, are slightly thinner than those in the non-heating case affected by the evaporation, their distribution is almost the same as for those in the unheated case. Similar trends are also seen in the probability density function of the wave height in Figure 10-2, compared with those in the unheated case shown in Figure 10-1.

On the other hand, the wave frequency $f$, shown in Figure 11-2, is nearly doubled compared with that in the unheated case. This is also the case of the disturbance wave frequency $f_{DW}$, shown in Figure 12. From these Figures, it is clear that the liquid film surface easily becomes wavy, when the wall heat flux is increased.

The distribution of the local heat transfer coefficient $\alpha$ in the case of a higher heat flux is shown in Figure 15-2. In the region of $x/D>40$, $\alpha$ increases slightly with distance, different from its counterpart of the low heat flux case.

## 4. ANALYSIS WITH SURFACE RENEWAL MODEL

In order to explain qualitatively the enhancement of heat transfer by the onset of disturbance waves, an analysis has been carried out with a surface renewal model. To simplify the problem, the developed state has been assumed both for the averaged velocity and the averaged temperature distributions in the liquid film. Also, the flow inside the liquid film is assumed to be two-dimensional because it is thin.

Inside the disturbance wave, a kind of circular motion may be expected, as reviewed by Dukler[20]. This circular motion may aid the heat transport inside the

waves. Consequently, the temperature may be considered to be distributed almost uniformly inside the disturbance waves. Therefore, it may be reasonable to expect that the temperature distribution becomes uniform at the instant when the disturbance wave passes a certain point. Later, it will recover gradually toward that of a 'developed' state. This type of change in the temperature distribution in the liquid film may happen nearly periodically with the frequency $f_{DW}$.

The above picture may not differ so much from an actual case, because the time duration $\Delta t_{DW}$ when a point on the wall surface is swept by a disturbance wave is much less than the period $1/f_{DW}$. In fact, defining $\Delta t_{DW}$ as the time difference between when the time derivative of the film thickness-time record exceeds the threshold, mentioned before, and when it becomes zero after its large negative value, $\Delta t_{DW}/(1/f_{DW})$ is found to be less than 0.1.

Based on the above picture, a surface renewal model[21] was applied to this change of temperature distribution in the liquid film. In this model, the equation of energy for the liquid film near the wall reduces to

$$\frac{\partial T}{\partial t}=a\frac{\partial^2 T}{\partial y^2} \tag{1}$$

where $T$ is the temperature in the liquid film, $a$ the thermal diffusivity, $t$ the time and $y$ the distance from the pipe wall. Let the moment when the temperature distribution is made uniform be the origin of the time coordinate. The initial condition yields

$$\theta=\theta_M=T_w-T_M \quad \text{for } y>0, \text{ at } t=0 \tag{2}$$

where $\theta=T_w-T$ is the temperature difference and $T_M$ is the uniform temperature, which is assumed to be equal to the bulk temperature of the liquid film. Because of the large heat capacity of the pipe wall, the inner-wall temperature is insensitive to the change of temperature distribution in the liquid film near the wall. That is, the boundary condition at the wall may be written as

$$\theta=T_w-T=0 \quad \text{for } y=0, \text{ at } t>0 \tag{3}$$

The solution of equation (1) under these conditions is

$$\theta=\theta_M \mathrm{erf}\{y/2(at)^{1/2}\} \tag{4}$$

where erf means error function.

The total heat flux $q_w$ transferred to the liquid film is assumed to consist of two independent parts:

$$q_w=q_{DW}+q_R \tag{5}$$

where $q_R$ is the basic heat flux supplied to the liquid film, irrespective of the onset of a disturbance wave. It may be equivalent to the heat flux of a ripple condition.

The additional heat flux $q_{DW}$ can be obtained by integrating the instantaneous heat flux due to the change in the temperature distribution caused by the disturbance waves. It is evaluated from the following equation.

$$q_{DW}=\frac{1}{\overline{t_{DW}}}\int^{\overline{t_{DW}}}\lambda\frac{\partial\theta}{\partial y}\bigg|_{y=0}dt=\frac{2\lambda(T_w-T_M)}{(\pi a t_{DW})^{1/2}} \tag{6}$$

where $\lambda$ is the thermal conductivity of the liquid phase.

The bulk temperature in equation (6) is determined by a laminar flow approxim-ation for the liquid film. That is, the developed laminar distribution may be achieved at each end of the period of the renewal action. The velocity distribution becomes

$$U^+=y^+ \tag{7}$$

where $U^+=U/(\tau_w/\rho_l)^{1/2}$ is the dimensionless streamwise velocity and $y^+=y(\tau_w/\rho_l)^{1/2}/\nu$ is the dimensionless distance from the pipe wall. Almost all the heat flux may be transferred to the gas phase flow through the developed liquid film. Hence, the temperature distribution in the liquid film becomes

$$T^+=Pr\cdot y^+ \tag{8}$$

where $T^+=\rho_l c_{pl}(\tau/_w\rho_l)^{1/2}/q_R$ is the dimensionless temperature, $c_{pl}$ the specific heat at constant pressure and $Pr$ the Prandtl number. The dimensionless bulk temperature is defined as follows;

$$T_M^+=\frac{\rho_l c_{pl}(T_w-T_M)(\tau_w/\rho_l)^{1/2}}{q_R}=\int_0^{\delta^+}T^+u^+dy^+/\int_0^{\delta^+}u^+dy^+ \tag{9}$$

where $\bar{\delta}^+=\bar{\delta}(\tau_w/\rho_l)^{1/2}/\nu$ is the dimensionless mean film thickness. Substituting equations (7), (8) and (9) into equation (6), $q_{DW}$ yields

$$q_{DW}=\frac{4q_R\bar{\delta}}{3(\pi a\overline{t_{DW}})^{1/2}} \tag{10}$$

The heat transfer coefficient $\alpha_{DW}$ of the disturbance wave flow regime is defined as follows;

$$\alpha_{DW}=\frac{q_{DW}+q_R}{T_w-T_{CL}}=\frac{q_R}{T_w-T_{CL}}\left(1+\frac{4\bar{\delta}}{3(\pi a\overline{t_{DW}})^{1/2}}\right) \tag{11}$$

Experimental results have been substituted into the value of $q_R$, $T_w-T_{CL}$ and $\overline{t_{DW}}=1/f_{DW}$, obtained at $X=1200$ mm.

The calculated results of $\alpha_{DW}$ are shown as the ratio of $\alpha_{DW}/\alpha_R$ in Table 1, and compared with the experimental values. Here, $\alpha_R$ denotes the heat transfer coefficient obtained at a flow rate condition in a ripple wave flow regime. The enhancement of the heat transfer coefficient may have been explained.

Table 1 Ratio of $\alpha_{EW}/\alpha_E$

| | | Low heat flux | | | | | | High heat flux | |
|---|---|---|---|---|---|---|---|---|---|
| $G_E$ (g/sec.) | | 21.1 | | 15.5 | | 11.5 | | 15.5 | 11.5 |
| $G_l$ (g/sec.) | | 10.0 | 11.7 | 10.0 | 11.7 | 10.0 | 11.7 | 11.7 | 11.7 |
| $\frac{\alpha_{DW}}{\alpha_E}$ | Exp. | 1.40 | 1.50 | 1.43 | 1.56 | 1.50 | 1.69 | 1.47 | 1.31 |
| | Analysis | 1.45 | 1.49 | 2.25 | 2.45 | 2.39 | 2.87 | 2.20 | 2.10 |

## 5. CONCLUSIONS

An experimental study was performed on heat transfer and liquid film flow behaviour in an annular-mist two-phase two component flow. The instantaneous liquid film thickness was obtained by the conductance method. The main results obtained in this study are as follows;

(1) The enhancement of the heat transfer coefficient is found to correspond to the onset of a disturbance wave. It can also be explained qualitatively, applying the surface renewal model to the temperature distribution of a disturbance wave flow.

(2) The frequency of a disturbance wave increases with apparent gas phase velocity and with wall heat flux. The velocity of a disturbance wave also increases with apparent gas phase velocity, regardless of its height.

(3) Liquid film surface easily becomes wavy, when the wall heat flux increases.

### References


1) A. S. Telles and A. E. Dukler; Indust. Eng. Chem. Fundam., **9**, 412 (1970)
2) K. J. Chu and A. E. Dukler; AIChE J., **20**, 695 (1974)
3) T. V. Narasimhan and E. J. Davis; Indust. Eng. Chem. Fundam., **11**, 490 (1972)
4) G. H. Anderson et al.; Chem. Eng. Sci., **12**, 109 (1960)
5) E. J. Davis et al.; AIChE J., **21**, 872 (1975)
6) V. M. Kozlov et al.; Proceedings 6th Intn'l Conf. on Heat Transfer **1**, 487 (1978)
7) T. Ueda and H. Tanaka; Int. J. Multiphase Flow, **2**, 261 (1975)
8) H. A. Johnson and A. H. Abou-Sabe; Trans. ASME, 977 (1952)
9) H. Groothuis and W. P. Handal; Chem. Eng, Sci., **11**, 212 (1959)
10) A. A. Kudirka et al. ; Indust. Eng. Chem. Fundam., **1**, 339 (1965)
11) R. H. Pletcher and H. N. McManus; Int. J. Heat and Mass Transfer, **11**, 1087 (1968)
12) H. N. McManus and R. H. Pletcher; Int. J. Heat and Mass Transfer, **12**, 663 (1969)
13) Y. Hagiwara et al.; Multiphase Transport **1** (ed. by N. Vezirouglu) Hemisphere Pub. Co. p. 111 (1979)
14) R. C. Brown et al.; Canad. J. Chem. Eng., **56**., 754 (1978)
15) G. V. Tsiklauri et al.; Two-phase Momentum, Heat and Mass Transfer **1** (ed. by F. Durst et al.) Hemisphere Pub. Co. p. 357 (1979)
16) J P. Villeneuve and Y. Ouellet; Rev. Sci. Instrum., **49**, 1425 (1978)
17) S. F. Chien and W. Ibele; Trans. ASME **86**-C, 89 (1964)

18) R. M. Nedderman et al.; Chem. Eng. Sci., **18**, 661 (1963)
19) K. Sekoguchi et al.; Trans. Jpn. Soc. Mech. Eng., **39**, 313 (1973)
20) A. E. Dukler; Chem. Eng. Educ., **11**, 108 (1977)
21) F. G. van Dongen et al.; Int. J. Heat and Mass Transfer, **21**, 1099 (1978)